IEEE Access
Multidisciplinary : Rapid Review : Open Access Journal

Received 13 August 2024, accepted 4 September 2024, date of publication 6 September 2024, date of current version 17 September 2024.

*Digital Object Identifier 10.1109/ACCESS.2024.3455757*

RESEARCH ARTICLE

# Design of Robust $H_\infty$ Guaranteed Cost Controller of Quadrotor UAV for Set-Point Tracking

**BYEONGHWA LEE[1], DONGHO HYUN[2], JUWON KIM[3], (Member, IEEE), SEUNGHWAN LEE[2], (Member, IEEE), AND JAEPIL BAN[2,4], (Member, IEEE)**

[1]Department of Systems and Control Engineering, School of Engineering, Tokyo Institute of Technology, Tokyo 152-8550, Japan
[2]School of Electronic Engineering, Kumoh National Institute of Technology, Gumi 39177, Republic of Korea
[3]Department of Electrical and Computer Engineering, Inha University, Incheon 22212, Republic of Korea
[4]Department of Aeronautic, Mechanical, and Electronic Convergence Engineering, Kumoh National Institute of Technology, Gumi 39177, Republic of Korea

Corresponding authors: Jaepil Ban (jpban@kumoh.ac.kr) and Seunghwan Lee (shlee@kumoh.ac.kr)

This work was supported by the National Research Foundation of Korea (NRF) through Korean Government, Ministry of Science and Information and Communication Technology (MSIT) under Grant NRF-2022R1G1A1006262.

**ABSTRACT** This study proposes a robust $H_\infty$ guaranteed cost controller (RHGCC) and its design method for set-point tracking control of quadrotor unmanned aerial vehicle (UAV) considering both model uncertainties and external disturbances. To guarantee a certain level of optimal performance against the effects of model uncertainties and external disturbances such as wind gusts, the proposed RHGCC integrates the $H_\infty$ control method with guaranteed cost control. Furthermore, a linear matrix inequality (LMI)-based controller design condition is proposed, guaranteeing not only a certain level of linear quadratic (LQ) cost but also the upper bound of the disturbance attenuation level in terms of $H_\infty$ norm. The proposed RHGCC is designed for the position and attitude control of the quadrotor UAV, enabling both the position and attitude of quadrotor UAV to be robust against external disturbances. Simulation results validate the effectiveness of the proposed RHGCC and demonstrate that the proposed method outperforms conventional methods in reducing tracking errors against disturbances. Especially, the proposed method significantly reduces the $H_\infty$ norm and suppresses disturbances compared to conventional methods.

**INDEX TERMS** Linear matrix inequality, optimal control, quadrotor UAV, robust control, set-point tracking control.

## NOMENCLATURE

### ACRONYMS

| | |
|---|---|
| DOF | degrees of freedom. |
| LMI | linear matrix inequality. |
| LQR | linear quadratic regulator. |
| PID | proportional-integral-derivative. |
| RHGCC | robust $H_\infty$ guaranteed cost controller. |
| UAV | unmanned aerial vehicle. |

### SYMBOLS

| | |
|---|---|
| $\Delta A_i$, $\Delta B_{i1}$ | model uncertainties. |
| $\gamma_i$ | upper bound of $H_\infty$ norm of $i$-th closed-loop system. |
| $\mathbb{R}$ | set of real numbers. |
| $\mathcal{B}$ | body-fixed frame. |
| $\mathcal{I}$ | right-hand inertial frame. |
| $\mathcal{J}_i^{'}$ | upper bound of $\mathcal{J}_i$. |
| $\mathcal{J}_i$ | LQ cost of $i$-th closed-loop system. |
| $\mathcal{R}$ | rotation matrix. |
| $\mu_i$ | virtual control inputs. |
| $\phi, \theta, \psi$ | roll, pitch, and yaw angles. |
| $\Pi$ | position vector. |
| $\Pi_d$, $\Theta_d$ | desired position and angle vectors. |
| $\star$ | transposed off-diagonal elements of a symmetric matrix. |
| $\tau_i$ | torques in the roll, pitch and yaw directions. |
| $E\{\cdot\}$ | expectation operator. |
| $tr\{\cdot\}$ | trace of $\cdot$. |
| $\Theta$ | angle vector. |
| $A_i, B_{i1}, B_{i2}, C_{zi}$ | system matrices. |

The associate editor coordinating the review of this manuscript and approving it for publication was Jianxiang Xi.

| | |
|---|---|
| $b$ | constant speed-to-force coefficient. |
| $C(\cdot)$ | cosine of $\cdot$. |
| $c$ | constant force-to-moment inertia. |
| $d_i(t)$ | time varying disturbances. |
| $D_i$ | damping matrices consisting of drag coefficients. |
| $diag(\cdot)$ | block diagonal matrix of $\cdot$. |
| $e_i$ | error state variables. |
| $f_i$ | lift forces. |
| $g$ | gravitational acceleration. |
| $J_x, J_y, J_z$ | moment of inertia. |
| $K_i$ | state feedback gains. |
| $k_x, k_y, k_z, k_\phi, k_\theta, k_\psi$ | nominal values of drag coefficient. |
| $l$ | distance between the center of gravity and rotor. |
| $m$ | mass of the quadrotor UAV. |
| $S(\cdot)$ | sine of $\cdot$. |
| $T, M$ | torque and virtual control input vectors. |
| $u_1$ | total lift force. |
| $U_i$ | control input vectors of error state model. |
| $w_i$ | spin rates of motors. |
| $x, y, z$ | coordinates for representing Euclidean positions. |
| $X_{ei}$ | error state vectors. |
| $z_i(t)$ | controlled outputs. |
| $\|\cdot\|_2$ | $\mathcal{L}_2$-norm of $\cdot$. |

## I. INTRODUCTION

Quadrotor unmanned aerial vehicles (UAVs) have gained much attention in recent years owing to their unique attributes, characterized by a simple structure and maneuverability, including vertical take-off and hover capabilities [1], [2]. Furthermore, in contrast to alternative airborne platforms, quadrotor UAVs manifest notable advantages in terms of weight efficiency, cost-effectiveness, and enhanced accessibility. These inherent characteristics have led to their widespread adoption across diverse domains, spanning education, military, agriculture, cargo and passenger transportation, surveillance, and simultaneous localization and mapping (SLAM) [3], [4], [5], [6], [7], [8].

In order for quadrotor UAVs to effectively operate within these diverse applications, their ability to navigate autonomously with high precision is crucial. In this context, extensive studies have been conducted on the control methods of quadrotor UAVs, including path-tracking control methods [9], [10] and set-point tracking control methods [11], [12]. However, designing a controller for quadrotor UAVs still faces multiple challenges due to the inherent nonlinearity of their models and the underactuated property [13], [14]. To overcome these challenges, previous studies have proposed a control framework that decomposes the system into two distinct subsystems: position control for translational motion and attitude control for rotational motion [12], [13], [15], [16], [17], [18]. In the framework, the original nonlinear dynamics are decomposed into linearized position and control models, augmented by a nonlinear coupling term. The hierarchical nature of this approach not only resolves the underactuated dynamics but also provides opportunities for developing systematic and straightforward controller design methodologies.

In addition, the model uncertainties and external disturbances are the main factors degrading the control performance of quadrotor UAVs. The model uncertainties can arise from inaccuracies in measurements and internal parameters such as aerodynamic coefficients and moments of inertia. Furthermore, owing to their relatively small and lightweight platform, quadrotor UAVs are sensitive to disturbances, such as wind gusts. Hence, it is crucial to consider these factors in designing the controller of quadrotor UAVs to achieve desired control objectives [1], [19]. Furthermore, to achieve control objectives in real-world applications such as cooperation with multiple unmanned systems, including quadrotor UAVs, it is necessary to consider constraints such as finite-time convergence, input saturation constraints, and discrete communication. These constraints can be overcome by introducing methods such as event-triggered control and neural network control [20], [21], [22], [23]. In this paper, we focus on control methods that minimize the impact of model uncertainties and disturbances among various constraints for the effective control of quadrotor UAV.

Various studies have investigated robust control methods employing the hierarchical control structure to achieve the desired control performance against model uncertainties and external disturbances [13], [19], [24], [25]. For example, [13] employed the robust integral of the signum of the error method for the inner-loop attitude control to reject disturbances, and an immersion and invariance-based adaptive control method was applied for the outer-loop position control to compensate for uncertainties. Reference [19] integrated adaptive control with PD-like control for both position and attitude control, demonstrating its robustness to both model uncertainties and disturbances without relying on a known upper bound. In [24], a robust generalized dynamic inversion was used for the inner loop to control horizontal positions, and adaptive non-singular terminal sliding mode control was employed for the outer loop to control vertical position, tilting angles (roll, pitch), and yaw angle. While these approaches succeeded in enhancing the robustness of the platform to disturbances and model uncertainties in the tracking control of quadrotor UAV, they did not consider achieving optimal control performance.

Meanwhile, optimal control methods have been investigated for position and attitude control, aiming to optimize a predefined performance index in the operation of quadrotor UAV [12], [15], [26], [27]. For example, in [26], an efficient nonlinear MPC using the improved continuation and generalized minimal residual algorithm was proposed for tracking control of quadrotor UAV. Reference [27] incorporated a feed-forward neural network as the prediction model, presenting a strategy to adaptively learn the model parameters using neural networks when exact model parameters are unknown. Although the aforementioned MPC-based strategies can implicitly reduce the effect of the model uncertainties, it is difficult to analyze the control performance of the proposed controller rigorously because model uncertainties and disturbances are not explicitly considered in the controller design. Furthermore, MPC strategies demand significant computational resources as they solve optimization problems and update control inputs at every step. In [15], a linear quadratic regulator (LQR) was adopted for both position and attitude control. However, this study did not consider model uncertainties in the controller design. In [12], guaranteed cost control (GCC) was applied for fixed-point tracking position and attitude control, incorporating model uncertainties. However, the study did not address the effect of external disturbances.

In this study, we propose the robust $H_\infty$ guaranteed cost control (RHGCC). The proposed control strategy integrates optimal control with $H_\infty$ control to achieve both optimal control performance and attenuation of the effects of model uncertainties and external disturbances. Specifically, the proposed RHGCC guarantees a certain level of the LQ cost and an upper bound on the $H_\infty$ norm against external disturbances to the controlled outputs. Both norm-bounded model uncertainties and external disturbances are explicitly modeled in the error state space equation. Subsequently, the performance analysis condition for a closed-loop error system is provided in terms of matrix inequality, guaranteeing the upper bound of the LQ cost and disturbance attenuation level. Then, based on the analysis condition, a linear matrix inequality (LMI)-based controller design condition is proposed, enabling the optimal controller gain to be obtained by solving a convex optimization problem. In particular, the proposed method considers both norm-bounded model uncertainties and external disturbances in the optimal controller design, whereas the existing studies ignored external disturbances when designing. The optimal performance and robustness of the proposed method are analyzed and verified through various simulations, and the results demonstrate the effectiveness of the proposed method in reducing disturbances. The qualitative comparison between the proposed and existing methods is summarized in Table 1. In addition, the major contributions of this study are summarized as follows:

- Model uncertainties are explicitly modeled in the tracking error state space equation of quadrotor UAV using norm-bounded uncertainties. Additionally, external disturbances are also modeled explicitly in the equation. Both modeled uncertainties and external disturbances are considered in the performance analysis and controller design of quadrotor UAV.
- A performance analysis condition for a closed-loop system is provided in terms of matrix inequalities, guaranteeing the upper bound of the LQ cost and disturbance attenuation level simultaneously. Based on the analysis, an LMI-based controller design condition is proposed, enabling the optimal RHGCC gain to be obtained by solving a convex optimization problem.
- Simulations are conducted in various scenarios, characterized by instantaneous, continuous, and complex disturbances. Furthermore, a comprehensive evaluation of the proposed RHGCC is conducted to demonstrate its effectiveness in reducing disturbances through comparative analysis with conventional methods.

This paper is organized as follows: In section II, we present the linear modeling of a cascaded position and attitude control system for a quadrotor UAV. In section III, the design of RHGCC for set-point tracking control is presented. In section IV, simulations and performance analysis are conducted under various disturbance scenarios. Finally, section V concludes the paper.

**TABLE 1. Qualitative comparison with existing studies on quadrotor UAV.**

| Ref | LQ Cost | Model Uncertainty | $H_\infty$ Control | Tracking Control | LMI-based Design |
|---|---|---|---|---|---|
| **Proposed** | **O** | **NU** | **O** | **SP** | **O** |
| [9] | O | NC | NC | PT | X |
| [10] | X | NU | NC | PT | X |
| [11] | X | NC | NC | SP | X |
| [12] | O | NU | NC | SP | O |
| [13] | X | NC | NC | PT | X |
| [14] | X | NC | NC | PT | X |
| [15] | O | NC | NC | PT | X |
| [16] | X | NC | NC | PT | X |
| [17] | X | NC | NC | SP, PT | X |
| [18] | X | NC | NC | SP, PT | X |
| [19] | X | NU | NC | PT | X |
| [24] | X | NC | NC | PT | X |
| [25] | X | NC | NC | SP, PT | X |
| [26] | O | NC | NC | PT | X |
| [27] | O | NC | NC | PT | X |

BMI: bilinear matrix inequality, LQ: linear quadratic,
LMI: linear matrix inequality, NU: norm-bounded uncertainty,
NC: not considered, SP: set point tracking, PT: path tracking.

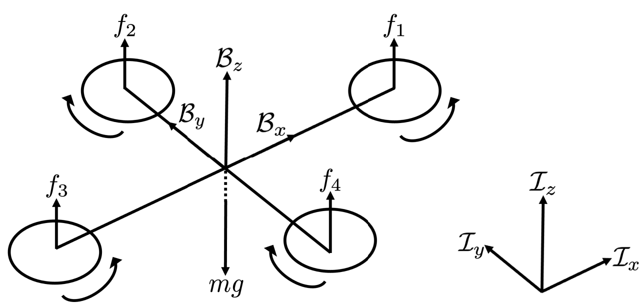


**FIGURE 1. Schematics of quadrotor UAV.**

## II. PROBLEM FORMULATION

In this study, we consider the quadrotor UAV consisting of four rotors, with two rotors facing each other rotating clockwise or counterclockwise (Fig. 1) [13]. These four rotors generate the lift forces of the quadrotor UAV, denoted by

$$f_i(t) = bw_i^2,\ i \in \{1, \cdots, 4\}. \tag{1}$$

$\mathcal{I} = \{\mathcal{I}_x, \mathcal{I}_y, \mathcal{I}_z\}$ represents a right-hand inertial frame in the 3-dimensional space, and $\mathcal{B} = \{\mathcal{B}_x, \mathcal{B}_y, \mathcal{B}_z\}$ represents the body-fixed frame, respectively, where its origin is the center of gravity. The Euclidean position of the quadrotor UAV is represented as $\Pi(t) = [x(t), y(t), z(t)]^T$ in the inertial frame, and $\Theta(t) = [\phi(t), \theta(t), \psi(t)]^T$ denotes the Euler angle of the quadrotor UAV, respectively. In addition, the rotation matrix $\mathcal{R}$ from $\mathcal{B}$ to $\mathcal{I}$ is expressed as follows [18]:

$$\mathcal{R} = \begin{bmatrix} C\phi C\theta & S\phi S\theta C\psi - C\phi S\psi & C\phi S\theta C\psi + S\phi S\psi \\ S\phi C\theta & S\phi S\theta S\psi + C\phi C\psi & C\phi S\theta S\psi - S\phi C\psi \\ -S\theta & C\theta S\phi & C\phi C\theta \end{bmatrix}. \tag{2}$$

The dynamics of the translational and rotational motions of the quadrotor UAV can be represented as:

$$m\ddot{\Pi}(t) + D_1\dot{\Pi}(t) + G = B_1 u_1(t) + d_1(t), \tag{3}$$
$$J\ddot{\Theta}(t) + LD_2\dot{\Theta}(t) = B_2 T(t) + d_2(t), \tag{4}$$

where

$$J = diag(J_x, J_y, J_z),$$
$$D_1 = diag(k_x, k_y, k_z), \quad D_2 = diag(k_\phi, k_\theta, k_\psi),$$
$$G = \begin{bmatrix} 0 \\ 0 \\ mg \end{bmatrix}, \quad L = diag(l, l, 1),$$
$$B_1 = \begin{bmatrix} C\phi S\theta C\psi \ + S\phi S\psi \\ C\phi S\theta S\psi \ - S\phi C\psi \\ C\phi C\theta \end{bmatrix}, \quad B_2 = diag(l, l, c),$$
$$T(t) = \begin{bmatrix} \tau_1(t) \\ \tau_2(t) \\ \tau_3(t) \end{bmatrix}, \quad d_1(t) = \begin{bmatrix} d_x(t) \\ d_y(t) \\ d_z(t) \end{bmatrix}, \ d_2(t) = \begin{bmatrix} d_\phi(t) \\ d_\theta(t) \\ d_\psi(t) \end{bmatrix}.$$

Here, $J$ denotes the moment of inertia in each direction. $D_1$ and $D_2$ are the damping matrices, which consist of the nominal values of drag coefficients. $B_1$ and $B_2$ are input gain matrices. $d_1(t)$ and $d_2(t)$ represent time-varying disturbances with respect to position and attitude, respectively. $u_1(t)$ denotes the total lift force. $T(t)$ denotes the rotation torque vector, including roll, pitch, and yaw torques. $u_1(t)$ and $T(t)$ are defined as:

$$\begin{aligned} u_1 &= f_1 + f_2 + f_3 + f_4, \\ \tau_1 &= -f_1 - f_2 + f_3 + f_4, \\ \tau_2 &= -f_1 + f_2 + f_3 - f_4, \\ \tau_3 &= f_1 - f_2 + f_3 - f_4. \end{aligned} \tag{5}$$

The desired values of the position and attitude of the quadrotor UAV are defined as $\Pi_d = [x_d, y_d, z_d]^T$ and $\Theta_d = [\phi_d, \theta_d, \psi_d]^T$, respectively. Then, the error state vectors are defined as:

$$\begin{aligned} &e_1(t) = \Pi(t) - \Pi_d,\ e_2(t) = \dot{\Pi}(t) - \dot{\Pi}_d, \\ &e_3(t) = \Theta(t) - \Theta_d,\ e_4(t) = \dot{\Theta}(t) - \dot{\Theta}_d. \end{aligned} \tag{6}$$

Defining the virtual control input $M(t) = [\mu_1(t), \mu_2(t), \mu_3(t)]^T$, we have from (3), (4), and (6):

$$\dot{e}_1(t) = e_2(t), \tag{7a}$$
$$\begin{aligned} \dot{e}_2(t) = &-\frac{1}{m}D_1 e_2(t) + M(t) - \frac{1}{m}D_1\dot{\Pi}_d - \ddot{\Pi}_d \\ &+ \frac{1}{m}d_1(t) + \left\{\frac{1}{m}B_1 u_1(t) - G - M(t)\right\}, \end{aligned} \tag{7b}$$
$$\dot{e}_3(t) = e_3(t), \tag{7c}$$
$$\begin{aligned} \dot{e}_4(t) = &J^{-1}\left\{LD_2 e_4(t) + B_2 T(t) - LD_2\dot{\Theta}_d + d_2(t)\right\} \\ &- \ddot{\Theta}_d, \end{aligned} \tag{7d}$$

where $\left\{\frac{1}{m}B_1 u_1(t) - G - M(t)\right\}$ is a coupling term that links position control and attitude control, and it can be eliminated from the state space equation by defining the elements in the virtual control input $M(t)$ as:

$$\begin{aligned} \mu_1(t) &= \frac{u_1(t)}{m}(C\phi_d S\theta_d C\psi_d + S\phi_d S\psi_d), \\ \mu_2(t) &= \frac{u_1(t)}{m}(C\phi_d S\theta_d S\psi_d - S\phi_d C\psi_d), \\ \mu_3(t) &= \frac{u_1(t)}{m}(C\phi_d C\theta_d) - g. \end{aligned} \tag{8}$$

Furthermore, $\dot{\Pi}_d$, $\ddot{\Pi}_d$, $\dot{\Theta}_d$ and $\ddot{\Theta}_d$ are zero since they are time-invariant values for set-point tracking control. Therefore, we have the following state space representation of the error dynamics from (7) and (8):

$$\dot{X}_{e1}(t) = A_1 X_{e1}(t) + B_{11}M(t) + B_{12}d_1(t), \tag{9}$$
$$\dot{X}_{e2}(t) = A_2 X_{e2}(t) + B_{21}T(t) + B_{22}d_2(t), \tag{10}$$

where

$$X_{e1}(t) = \begin{bmatrix} e_1(t) \\ e_2(t) \end{bmatrix}, \quad X_{e2}(t) = \begin{bmatrix} e_3(t) \\ e_4(t) \end{bmatrix},$$
$$A_1 = \begin{bmatrix} O_{3x3} & I_{3x3} \\ O_{3x3} & -\frac{1}{m}D_1 \end{bmatrix}, \quad A_2 = \begin{bmatrix} O_{3x3} & I_{3x3} \\ O_{3x3} & -J^{-1}LD_2 \end{bmatrix},$$
$$B_{11} = \begin{bmatrix} O_{3x3} \\ I_{3x3} \end{bmatrix}, \quad B_{12} = \frac{1}{m}\begin{bmatrix} O_{3x3} \\ I_{3x3} \end{bmatrix},$$
$$B_{21} = \begin{bmatrix} O_{3x3} \\ J^{-1}B_2 \end{bmatrix}, \quad B_{22} = \frac{1}{m}\begin{bmatrix} O_{3x3} \\ J^{-1} \end{bmatrix}.$$

From (8), the total lift force $u_1$ and desired values of roll and pitch, $\phi_d$ and $\theta_d$, are obtained as follows:

$$\begin{aligned} u_1 &= m\sqrt{\mu_1{}^2(t) + \mu_2{}^2(t) + \{\mu_3(t) + g\}^2}, \\ \phi_d &= \arcsin\left[\frac{m}{u_1(t)}\{\mu_1(t)S\psi_d - \mu_2(t)C\psi_d\}\right], \\ \theta_d &= \arctan\left[\frac{1}{\mu_3(t) + g}\{\mu_1(t)C\psi_d + \mu_2(t)S\psi_d\}\right]. \end{aligned} \tag{11}$$

Fig. 2 shows the entire structure of the control system. The position control, forming the outer loop, and the attitude control, forming the inner loop, are linked by the nonlinear decoupling equations (11). We assume that the matrices

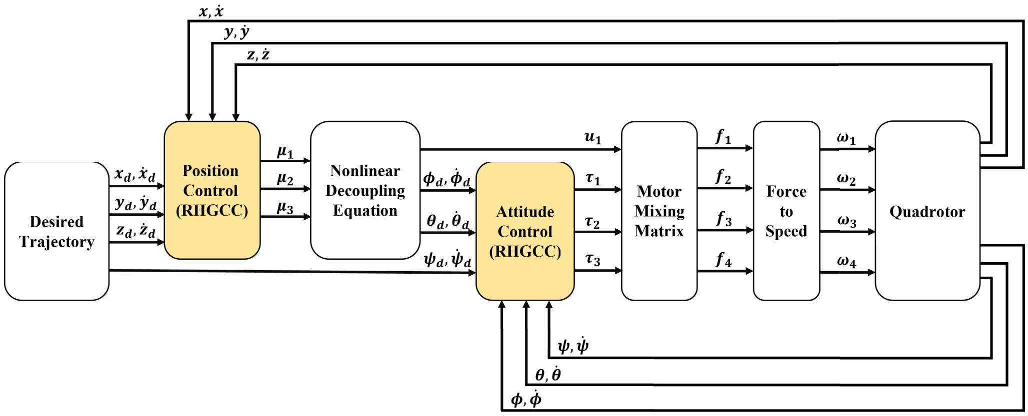


**FIGURE 2.** The entire control system structure for quadrotor UAV: In this structure, position control and attitude control are linked in a cascade by the nonlinear decoupling equation.

$(A_1, B_{11}, A_2, B_{21})$ have norm-bounded model uncertainties as:

$$A_1 = A_{10} + \Delta A_1,\ B_{11} = B_{110} + \Delta B_{11},$$
$$A_2 = A_{20} + \Delta A_2,\ B_{21} = B_{210} + \Delta B_{21}, \tag{12}$$

where

$$\Delta A_1 = S_1 F(t) E_1,\ \Delta B_{11} = S_1 F(t) E_3,$$
$$\Delta A_2 = S_2 F(t) E_2,\ \Delta B_{21} = S_2 F(t) E_4. \tag{13}$$

Here, $S_1, S_2 \in \mathbb{R}^{6\times 3}$, $E_1, E_2 \in \mathbb{R}^{3\times 6}$ and $E_3, E_4 \in \mathbb{R}^{3\times 3}$ are given constant matrices representing the structure of uncertainties. Additionally, $F(t) \in \mathbb{R}^{n\times n}$ consists of Lebesgue measurable elements satisfying the following condition:

$$F^T(t)F(t) \leq I. \tag{14}$$

Thus, (9) and (10) can be rewritten as:

$$\dot{X}_{e1}(t) = (A_{10} + \Delta A_1)X_{e1}(t) + (B_{110} + \Delta B_{11})M(t) + B_{12}d_1(t), \tag{15}$$
$$\dot{X}_{e2}(t) = (A_{20} + \Delta A_2)X_{e2}(t) + (B_{210} + \Delta B_{21})T(t) + B_{22}d_2(t). \tag{16}$$

In addition, (15) and (16) can be simply expressed as follows:

$$\dot{X}_{ei}(t) = (A_{i0} + \Delta A_i)X_{ei}(t) + (B_{i10} + \Delta B_{i1})U_i(t) + B_{i2}d_i(t), \quad i \in \{1, 2\}. \tag{17}$$

The LQ cost function of each control system is represented as follows:

$$\mathcal{J}_i(X_{ei}(t), U_i(t)) = \int_0^\infty \left\{ X_{ei}^T(t) Q_i X_{ei}(t) + U_i^T(t) R_i U_i(t) \right\} dt, \quad i \in \{1, 2\}, \tag{18}$$

where $\mathcal{J}_i$ is a positive scalar. $Q_i$ and $R_i$ are given positive-definite symmetric matrices, respectively. Furthermore, for a positive scalar $\gamma_i (i \in \{1, 2\})$, the upper bounds of $H_\infty$ norm of each subsystem are represented as follows:

$$\frac{\|z_i(t)\|_2}{\|d_i(t)\|_2} < \gamma_i, \ i \in \{1, 2\}, \tag{19}$$

where $d_i(t)$ represents time-varying disturbances. The controlled output $z_i(t)$ is represented as $z_i(t) = C_{zi}X_{ei}(t)$, where $C_{zi}$ is a given constant matrix with appropriate dimension. Now, we define the RHGCC of the system (17) as follows.

*Definition 1:* The control law $U_i(t)$ is said to be the RHGCC of the system (17) if the control law $U_i(t)$ guarantees that the system (17) is stable and satisfies (19) for $d_i(t) \neq 0$ and $\mathcal{J}_i' \geq \mathcal{J}_i(X_{ei}(t), U_i(t))$ for $d_i(t) = 0$ for positive scalars $\gamma_i$ and $\mathcal{J}_i'$.

This study aims to find the state feedback gain $K_i$ of the controller $U_i(t) = K_i X_{ei}(t)$ that achieves the RHGCC of the system (17).

## III. ROBUST $H_\infty$ GUARANTEED COST CONTROLLER DESIGN

In this section, the design of the RHGCC for position and attitude control of the proposed quadrotor UAV is presented. The following theorem presents the matrix inequality condition to obtain the state feedback controller gains $K_i$ of RHGCC.

*Theorem 1:* Consider the system (17). The control law $U_i(t) = K_i X_{ei}(t)$ is said to be RHGCC if there exists a positive-definite matrix $P_i$ and positive scalars $\epsilon_{ij} (i \in \{1, 2\}, j \in \{1, \cdots, n\})$ for the given positive scalar $\gamma_i$ such that

$$Q_i + K_i^T R_i K_i + P_i(A_{i0} + B_{i10}K_i) + (A_{i0} + B_{i10}K_i)^T P_i + (S_i\bar{M}_i)\bar{M}_i^{-1}(S_i\bar{M}_i)^T + \bar{E}_i^T \bar{M}_i \bar{E}_i + \gamma_i^{-2} P_i B_{i2} B_{i2}^T P_i + C_{zi}^T C_{zi} < 0, \tag{20}$$

where $\bar{E}_i = E_i + E_{i+2}K_i$ and $\bar{M}_i = diag(\epsilon_{i1}, \cdots, \epsilon_{in})$. In addition, the upper bound of the LQ cost $\mathcal{J}_i'$ is calculated as $X_{ei0}^T P_i X_{ei0}$, where $X_{ei0}$ is an initial value of the $X_{ei}(t)$ at $t = 0$.

*Proof:* Substituting the input $U_i(t) = K_iX_{ei}(t)$ into (17), we have:

$$\dot{X}_{ei}(t) = (A_{i0} + B_{i10}K_i + \Delta A_i + \Delta B_{i1}K_i)X_{ei}(t) + B_{i2}d_i(t),\ i \in \{1, 2\}. \tag{21}$$

Define the Lyapunov function candidate as:

$$V(X_{ei}(t)) = X_{ei}^T(t)P_iX_{ei}(t). \tag{22}$$

Then, the time derivative of (22) along (17) can be calculated as:

$$\begin{aligned}\dot{V}(X_{ei}(t)) = &X_{ei}^T(t)[P_i\{(A_{i0} + B_{i10}K_i) + S_iF_i\bar{E}_i\} \\ &+ \{(A_{i0} + B_{i10}K_i) + S_iF_i\bar{E}_i\}^T P_i]X_{ei}(t) \\ &+ X_{ei}^T(t)P_iB_{i2}d_i(t) + d_i^T(t)B_{i2}^TP_iX_{ei}(t).\end{aligned} \tag{23}$$

By Lemma 1 [28], (23) can be rewritten as follows:

$$\begin{aligned}\dot{V}(X_{ei}(t)) \leq &X_{ei}^T(t)[P_i(A_{i0} + B_{i10}K_i)(A_{i0} + B_{i10}K_i)^TP_i \\ &+ (P_iS_i\bar{M}_i)\bar{M}_i^{-1}(P_iS_i\bar{M}_i)^T + \bar{E}_i^T\bar{M}_i^{-1}\bar{E}_i \\ &+ \gamma_i^{-2}P_iB_{i2}B_{i2}^TP_i]X_{ei}(t) + \gamma_i^2d_i^T(t)d_i(t).\end{aligned} \tag{24}$$

From (20) and (24), we have

$$\begin{aligned}\dot{V}(X_{ei}(t)) \leq &X_{ei}^T(t)[P_i(A_{i0} + B_{i10}K_i)(A_{i0} + B_{i10}K_i)^TP_i \\ &+ (P_iS_i\bar{M}_i)\bar{M}_i^{-1}(P_iS_i\bar{M}_i)^T + \bar{E}_i^T\bar{M}_i^{-1}\bar{E}_i \\ &+ \gamma_i^{-2}P_iB_{i2}B_{i2}^TP_i]X_{ei}(t) + \gamma_i^2d_i^T(t)d_i(t) \\ < &X_{ei}^T(t)\{-Q_i - K_i^TR_iK_i - C_{zi}^TC_{zi}\}X_{ei}(t) \\ &+ \gamma_i^2d_i(t)^Td_i(t).\end{aligned} \tag{25}$$

First, for $d_i(t) = 0$, (25) can be rewritten as:

$$\begin{aligned}\dot{V}(X_{ei}(t)) \leq &X_{ei}^T(t)[P_i(A_{i0} + B_{i10}K_i)(A_{i0} + B_{i10}K_i)^TP_i \\ &+ (P_iS_i\bar{M}_i)\bar{M}_i^{-1}(P_iS_i\bar{M}_i)^T + \bar{E}_i^T\bar{M}_i^{-1}\bar{E}_i \\ &+ \gamma_i^{-2}P_iB_{i2}B_{i2}^TP_i]X_{ei}(t) \\ < &X_{ei}^T(t)\{-Q_i - K_i^TR_iK_i - C_{zi}^TC_{zi}\}X_{ei}(t) \\ \leq &X_{ei}^T(t)\{-Q_i - K_i^TR_iK_i\}X_{ei}(t) < 0.\end{aligned} \tag{26}$$

Thus, the system (17) is asymptotically stable from (22) and (26). On the other hand, by integrating (26) from $t = 0$ to $\infty$, one can obtain:

$$\int_0^\infty \dot{V}(X_{ei}(t))\,dt < -\int_0^\infty X_{ei}^T(t)\{Q_i + K_i^TR_iK_i\}X_{ei}(t)\,dt. \tag{27}$$

As the system (17) is asymptotically stable, the $V(t)$ converges to zero as $t \to \infty$. Thus, by solving the integral in (27), we obtain:

$$V(X_{ei}(0)) = X_{ei}^T(0)P_iX_{ei}(0) = \mathcal{J}_i' > \mathcal{J}_i. \tag{28}$$

Therefore, the LQ cost $\mathcal{J}_i$ has the upper bound $\mathcal{J}_i'$. Next, for $d_i(t) \neq 0$, (25) can be rewritten as follows:

$$\begin{aligned}\dot{V}(X_{ei}(t)) < &X_{ei}^T(t)\{-Q_i - K_i^TR_iK_i - C_{zi}^TC_{zi}\}X_{ei}(t) \\ &+ \gamma_i^2d_i(t)^Td_i(t).\end{aligned} \tag{29}$$

Similarly, by integrating both sides of the inequality (29) from $t = 0$ to $\infty$, one can obtain:

$$\begin{aligned}\int_0^\infty \dot{V}(X_{ei}(t))\,dt < &\int_0^\infty X_{ei}^T(t)\{-Q_i - K_i^TR_iK_i\}X_{ei}(t)\,dt \\ &+ \int_0^\infty \{\gamma_i^2d_i(t)^Td_i(t) \\ &- X_{ei}^T(t)C_{zi}^TC_{zi}X_{ei}(t)\}\,dt < 0.\end{aligned} \tag{30}$$

Integrating (30) from $t = 0$ to $\infty$ yields

$$\begin{aligned}&V(X_{ei}(0)) + \int_0^\infty \{\gamma_i^2d_i(t)^Td_i(t) - X_{ei}^T(t)C_{zi}^TC_{zi}X_{ei}(t)\}dt \\ &> V(X_{ei}(\infty)) + \int_0^\infty X_{ei}^T(t)\{Q_i + K_i^TR_iK_i\}X_{ei}(t)\,dt > 0.\end{aligned} \tag{31}$$

For the initial value $X_{ei}(0) = 0$, we have from (31):

$$\int_0^\infty \{\gamma_i^2d_i(t)^Td_i(t) - X_{ei}^T(t)C_{zi}^TC_{zi}X_{ei}(t)\}dt > 0. \tag{32}$$

(32) can be rewritten as:

$$\gamma_i^2\int_0^\infty \|d_i(t)\|_2^2dt > \int_0^\infty \|z_i(t)\|_2^2dt, \tag{33}$$

where $\gamma_i$ is the upper bound of $\mathcal{L}_2$ gain from $d_i(t)$ to $z_i(t)$. This completes the proof. □

Note that the matrix inequalities in Theorem 1 are bilinear matrix inequalities (BMIs), which are nonconvex. Thus, obtaining solutions satisfying the inequalities is an NP-hard problem. Therefore, it is required to relax the BMI conditions in Theorem 1 to LMI conditions. Theorem 2 presents the controller design using the LMI conditions relaxed from the conditions in Theorem 1.

*Theorem 2:* The control law $U_i(t) = K_iX_{ei}(t)$ is said to be RHGCC if there exists a matrix $N_i = K_iP_i^{-1}$, positive definite matrices $H_i = P_i^{-1}$ and $Y_i$, and positive scalars $\epsilon_{ij}(i \in \{1, 2\}, j \in \{1, \cdots, n\})$ for given positive scalar $\gamma_i$ such that

$$\begin{bmatrix} A_{ci} & H_i & N_i^T & S_i\bar{M}_i & \bar{E}_i^T & H_iC_{zi}^T & B_{i2} \\ \star & -Q_i^{-1} & O & O & O & O & O \\ \star & \star & -R_i^{-1} & O & O & O & O \\ \star & \star & \star & -\bar{M}_i & O & O & O \\ \star & \star & \star & \star & -\bar{M}_i & O & O \\ \star & \star & \star & \star & \star & -I & O \\ \star & \star & \star & \star & \star & \star & -\gamma_i^2I \end{bmatrix} < 0, \tag{34}$$

$$\begin{bmatrix} Y_i & I \\ \star & H_i \end{bmatrix} \geq 0, \tag{35}$$

where $A_{ci} = A_{i0}H_i + B_{i10}N_i + (A_{i0}H_i + B_{i10}N_i)^T$, $\bar{E}_i = E_i + E_{i+2}K_i$, and $\bar{M}_i = diag(\epsilon_{i1}, \cdots, \epsilon_{in})$. In addition, the upper bound of the LQ cost $\mathcal{J}_i'$ is calculated as $X_{ei0}^TY_iX_{ei0}$, where $X_{ei0}$ is the initial value of $X_{ei}(t)$ at $t = 0$. Furthermore, the state feedback controller gain is calculated as $K_i = N_i H_i^{-1}$.

*Proof*: Pre- and post-multiplying (34) by $\Omega_i$ yields

$$\begin{bmatrix} \tilde{A}_{ci} & I & K_i^T & P_i S_i \bar{M}_i & P_i \bar{E}_i^T & C_{zi}^T & P_i B_{i2} \\ \star & -Q_i^{-1} & O & O & O & O & O \\ \star & \star & -R_i^{-1} & O & O & O & O \\ \star & \star & \star & -\bar{M}_i & O & O & O \\ \star & \star & \star & \star & -\bar{M}_i & O & O \\ \star & \star & \star & \star & \star & -I & O \\ \star & \star & \star & \star & \star & \star & -\gamma_i^2 I \end{bmatrix} < 0, \quad (36)$$

where $\Omega_i = diag\{H_i^{-1}, I, I, I, I, I, I\}$, $\tilde{A}_{ci} = P_i A_{i0} + P_i B_{i10} K_i + (P_i A_{i0} + P_i B_{i10} K_i)^T$, $N_i = K_i P_i^{-1}$, and $H_i = P_i^{-1}$, respectively. By applying the Schur complement, we have (20). In addition, applying the Schur complement to (35) yields

$$Y_i \geq H_i = P_i^{-1}. \quad (37)$$

Pre- and post-multiplying (37) by $X_{ei0}^T$ yields

$$X_{ei0}^T Y_i X_{ei0} \geq X_{ei0}^T P_i^{-1} X_{ei0}. \quad (38)$$

Thus, the upper bound of the LQ cost (18) for the system (17), $\mathcal{J}_i'$, is obtained as $X_{ei0}^T Y_i X_{ei0}$ in (38). This completes the proof. □

**TABLE 2. Parameters of the quadrotor UAV model used in the simulation.**

| Parameters | Values | Units |
|---|---|---|
| $m$ | 2.33 | kg |
| $g$ | 9.81 | m/s$^2$ |
| $J_x, J_y$ | 0.16 | kg·m$^2$ |
| $J_z$ | 0.32 | kg·m$^2$ |
| $k_x, k_y, k_z$ | 0.01 | N·s/m |
| $k_\phi, k_\theta, k_\psi$ | 0.012 | N·s/rad |
| $l$ | 0.4 | m |
| $c$ | 0.05 | - |

The optimal controller can be obtained by minimizing an upper bound of the LQ cost subject to the LMI condition in Theorem 2. Thus, we formulate a convex optimization problem to obtain the optimal controller. Assuming that $X_{ei0}$ is a zero mean random variable, i.e., $E\{X_{ei0} X_{ei0}^T\} = I$, we can obtain the following relation:

$$\begin{aligned} tr\{E\{\mathcal{J}_i\}\} &\leq tr\{E\{V(X_{ei}(0))\}\} = \mathcal{J}_i' \\ &\leq tr\{E\{X_{ei0}^T Y_i X_{ei0}\}\} \\ &\leq tr\{E\{X_{ei0} X_{ei0}^T\} Y_i\} = tr\{Y_i\}. \quad (39) \end{aligned}$$

Therefore, we can obtain the state feedback control gain $K_i$ minimizing the upper bound of the LQ cost $\mathcal{J}_i'$ by solving the following convex optimization problem:

$$\min_{\bar{M}_i, H_i, N_i, Y_i} \; tr\{Y_i\}$$
$$\text{subject to (34), (35).} \quad (40)$$

We can obtain the optimal state feedback gain by calculating $K_i = N_i H_i^{-1}$ from the solution of the optimization problem, achieving RHGCC.

*Remark 1:* Unlike the conventional designs of LQR and GCC, the design of the proposed RHGCC includes the upper bound of $H_\infty$ norm $\gamma_i$ as a constraint and solves an optimization problem that minimizes the LQ cost $\mathcal{J}_i'$ to obtain the optimal controller gain $K_i$. Therefore, it considers both the LQ optimal and $H_\infty$ control simultaneously, ensuring their upper bounds in the design. Particularly, since the quadrotor UAV model (17) explicitly includes model uncertainties and external disturbances, the controller is designed to obtain LQ optimal gains while achieving robustness against these uncertainties and disturbances.

*Remark 2:* Relaxing the BMI constraints to LMI conditions enables the optimal controller gain $K_i$ to be obtained by solving the convex optimization problem in (40), minimizing the upper bound of the LQ cost.

## IV. SIMULATION RESULTS

### A. PARAMETERS AND CONTROLLER GAINS

In this section, we show the effectiveness of the proposed RHGCC in reducing disturbances through simulations. The proposed RHGCC is compared with a conventional PID controller, a widely used control method, and an LQR, a representative optimal control method for linearized models. The parameters of the quadrotor UAV for the controller design and performance comparison are given in Table 2 [29]. In the simulations, the drag coefficients $k_x$, $k_y$, $k_z$, $k_\phi$, $k_\theta$, and $k_\psi$ are assumed to have a 30 percent perturbation, serving as the model uncertainties [12]. Thus, the uncertainty matrices $S_i$ and $E_i$ can be defined as follows:

$$S_1 = S_2 = \begin{bmatrix} O_{3\times3} \\ I_{3\times3} \end{bmatrix},$$

$$E_1 = \begin{bmatrix} 0 & 0 & 0 \\ 0 & 0 & 0 \\ 0 & 0 & 0 \\ 0.003 & 0 & 0 \\ 0 & 0.003 & 0 \\ 0 & 0 & 0.003 \end{bmatrix},$$

$$E_2 = \begin{bmatrix} 0 & 0 & 0 \\ 0 & 0 & 0 \\ 0 & 0 & 0 \\ 0.0036 & 0 & 0 \\ 0 & 0.0036 & 0 \\ 0 & 0 & 0.0036 \end{bmatrix},$$

$$E_3 = \begin{bmatrix} 0.1 & 0 & 0 \\ 0 & 0.1 & 0 \\ 0 & 0 & 0.1 \end{bmatrix}, \quad E_4 = \begin{bmatrix} 0.25 & 0 & 0 \\ 0 & 0.25 & 0 \\ 0 & 0 & 0.01562 \end{bmatrix}.$$

We set the matrices $Q_1 = Q_2 = I_{6\times6}$ and $R_1 = R_2 = I_{3\times3}$. We also set the matrices $C_{z1} = C_{z2} = I_{6\times6}$, assuming that every state is observable. In addition, we set $\gamma_1 = 0.5$ and $\gamma_2 = 25$. The following controller gains were obtained by solving the optimization problem (40) as:

$$K_1 = \begin{bmatrix} -4.7036 & 0 & 0 & -11.6509 & 0 & 0 \\ 0 & -4.7036 & 0 & 0 & -11.6509 & 0 \\ 0 & 0 & -4.7036 & 0 & 0 & -11.6509 \end{bmatrix},$$

$$K_2 = \begin{bmatrix} -1.4224 & 0 & 0 & -1.8038 & 0 & 0 \\ 0 & -1.4224 & 0 & 0 & -1.8038 & 0 \\ 0 & 0 & -3.0834 & 0 & 0 & -13.4687 \end{bmatrix}.$$

*Remark 3:* It is well known that the performance of the closed-loop response is affected by the choice of parameters $Q_1$, $Q_2$, $R_1$, $R_2$, $C_{z1}$, $C_{z2}$, $\gamma_1$, and $\gamma_2$. Specifically, $Q_1$ and $R_1$ are the weight parameters of the LQ cost for the position control. Each diagonal element of $Q_1$ is the weight for its corresponding state, while each diagonal component in $R_1$ is the weight for its corresponding control input. In other words, a large value of $Q_1$ exhibits the fast state response, whereas a large value of $R_1$ suppresses the magnitude of the control input. Similarly, $Q_2$ and $R_2$ serve the same function for attitude control. On the other hand, $C_{z1}$ and $C_{z2}$ determine the controlled outputs whose $\mathcal{L}_2$-gain over external disturbances are upper bounded by $\gamma_1$ and $\gamma_2$, respectively. Smaller values of $\gamma_1$ and $\gamma_2$ can result in better robustness to external disturbances but may lead to infeasible LMI conditions, requiring careful tuning.

**TABLE 3. Proportional, integral and differential gains of PID controllers.**

| | Proportional | Integral | Differential |
|---|---|---|---|
| Position | 0.8308 | 0.0081 | -0.0065 |
| Attitude | 0.6529 | 0.0339 | 2.8752 |

The PID gains of the conventional PID controller were obtained using the PID tuner in MATLAB (Table 3). In addition, the conventional LQR gains were obtained as:

$$K_{lqr,1} = \begin{bmatrix} 1.0000 & 0 & 0 & 1.7278 & 0 & 0 \\ 0 & 1.0000 & 0 & 0 & 1.7278 & 0 \\ 0 & 0 & 1.0000 & 0 & 0 & 1.7278 \end{bmatrix},$$

$$K_{lqr,2} = \begin{bmatrix} 1.0000 & 0 & 0 & 1.3297 & 0 & 0 \\ 0 & 1.0000 & 0 & 0 & 1.3297 & 0 \\ 0 & 0 & 1.0000 & 0 & 0 & 3.4826 \end{bmatrix}.$$

### B. SIMULATION 1: INSTANTANEOUS DISTURBANCES

In this subsection, we assess the quadrotor UAV's ability to hover when encountering a gust of wind after reaching the reference point. The initial input reference values are $\Pi_d = [5, 5, 5]^T$ m and $\Theta_d = [0, 0, 1.0472]^T$ rad. Namely, the quadrotor UAV is planned to rotate 60 degrees while moving to $[x, y, z]^T = [5, 5, 5]^T$ m from the origin initially. Note that these initial reference values for position and attitude were also used in the simulations conducted in the following subsections. The disturbances are applied as unit steps, as depicted in Fig. 3 and Fig. 6. First, Fig. 3 and Fig. 4 show the applied disturbances and the position control responses to them. For an air density of 1.2 kg/m$^3$ and a wind speed of 5 m/s, $F_w$ is calculated by 10 N, as $F_w = p_d A = \frac{1}{2}\rho v_w^2$, where $F_w$ is the wind force, $A$ is the surface area, $p_d$ is the dynamic pressure, $\rho$ is the density of air, and $v_w$ is the wind speed.

Fig. 4 depicts the responses when the disturbance $d_1(t)$ shown in Fig. 3 was applied in all $x$, $y$, and $z$ directions. At both 15 and 25 seconds, the position control response by the proposed method deviated by up to 0.15 m from the desired value. In contrast, the position control responses by the PID and LQR controllers deviated by up to 1.32 m and 0.85 m from the desired position, respectively. This indicates that the proposed RHGCC reduced the effect of disturbances by 88.6% and 82.4% compared to the PID control and LQR, respectively. From this simulation, it can be seen that the RHGCC's suppression of disturbances is much lower compared to the conventional PID and LQR controllers.

The $H_\infty$ norms of each controller were numerically calculated and shown in Fig. 5. The values of the $H_\infty$ norm of the PID and LQR controllers converged to 0.34 and 0.21, respectively, whereas that of the proposed RHGCC converged to 0.04, remaining within the initially given upper bound of $\gamma_1$. Therefore, the $H_\infty$ norm of the proposed RHGCC is 88.2% and 81.0% lower than those of the PID control and LQR, respectively, indicating that the proposed RHGCC significantly reduces the impact of disturbances compared to the conventional methods.

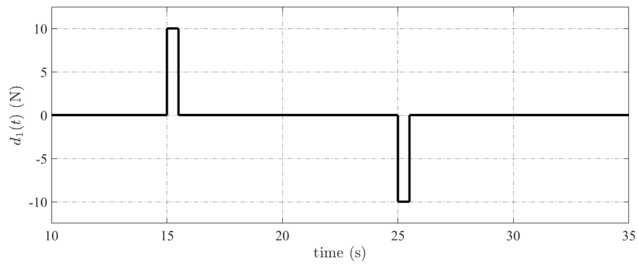


**FIGURE 3. Instantaneous disturbance inputs for position.**

Similarly, Fig. 7 shows the responses of attitude control when the disturbance of $\frac{\pi}{12}$ N·m at 30 seconds and $\frac{\pi}{15}$ N·m at 60 seconds is applied to the positive yaw angle (Fig. 6). Right after the first disturbance was applied, the attitude control responses by the PID control and LQR deviated by up to 0.67 rad and 0.46 rad from the desired yaw angle, respectively, whereas the response by proposed RHGCC deviated by up to 0.16 rad, reducing the effect of disturbances

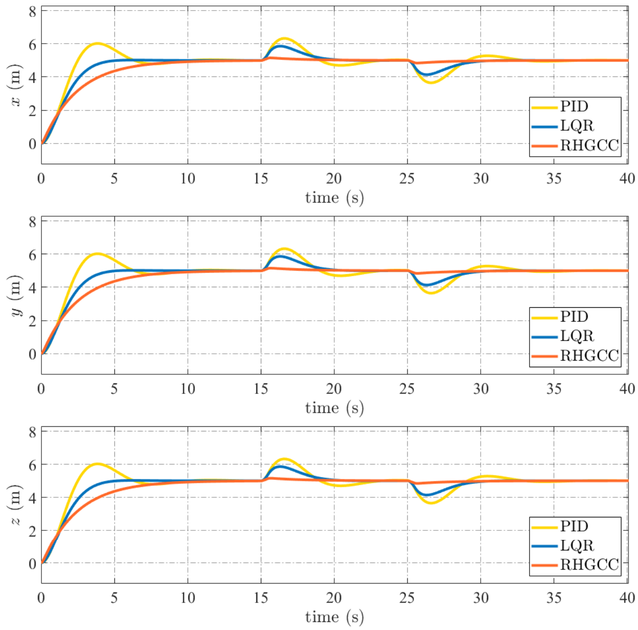


**FIGURE 4.** Responses of each controller for position tracking when disturbances in Fig. 3 are applied.

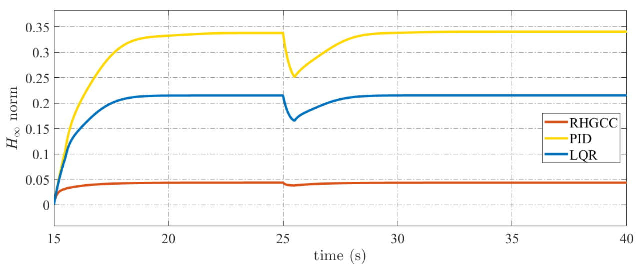


**FIGURE 5.** Calculated $H_\infty$ norms from responses in Fig. 4 for each controller.

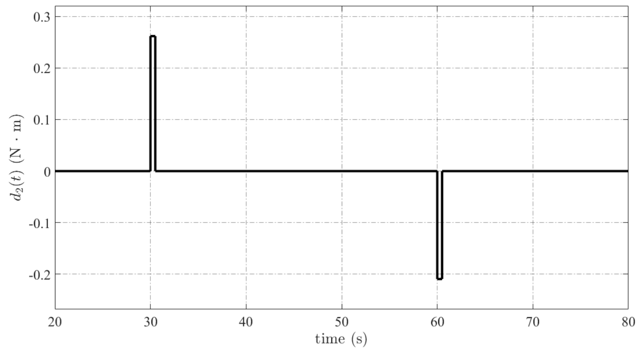


**FIGURE 6.** Instantaneous disturbance input for yaw angle in attitude.

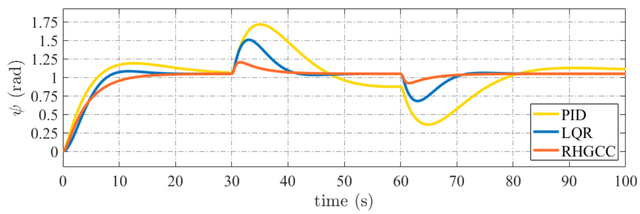


**FIGURE 7.** Responses of each controller for attitude tracking when disturbance in Fig. 6 is applied.

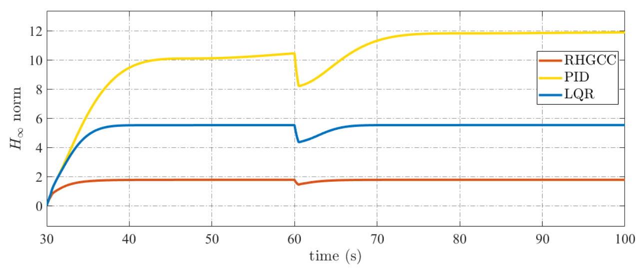


**FIGURE 8.** Calculated $H_\infty$ norms from responses in Fig. 7 for each controller.

by 76.1% and 65.2% compared to those of the PID and LQR controllers, respectively. Right after the second disturbance was applied, the responses of the PID control and LQR deviated by up to 0.69 rad and 0.37 rad from the desired yaw angle, respectively, whereas the response by proposed RHGCC deviated by up to 0.13 rad, reducing the effect of disturbances by 81.2% and 64.9% compared to those of the PID and LQR controllers, respectively.

In this simulation, the calculated $H_\infty$ norm values of each controller are compared in Fig. 8. The calculated $H_\infty$ norms of the PID control and LQR were approximately 11.9 and 5.5, respectively, whereas the calculated $H_\infty$ norm of the proposed RHGCC was approximately 1.8. This calculated $H_\infty$ norm of the proposed RHGCC remains below the initially given upper bound of $\gamma_2$, and is 84.9% and 67.3% lower than those of the PID and LQR controllers, respectively. Therefore, it can be concluded that the proposed RHGCC mitigated the impact of the disturbances and maintained proximity to the desired values compared to the conventional methods.

Meanwhile, when disturbances shown in Fig. 3 and Fig. 6 are not applied, the upper bounds of the LQ cost calculated by Theorem 2 for the given initial values are as follows:

$$\mathcal{J}_1' = 374.3217, \ \mathcal{J}_2' = 10.5538.$$

Fig. 9 shows the obtained LQ costs for each subsystem. The resulting LQ cost was 182.44 for $\mathcal{J}_1$ and 5.13 for $\mathcal{J}_2$. From this, we can verify that the LQ costs actually obtained are below their respective upper bounds.

### C. SIMULATION 2: CONTINUOUS DISTURBANCES

In this subsection, we compare the response and performance of each controller to continuously applied disturbances, while also examining the $H_\infty$ norm of each controller. The introduced disturbance $d_1(t)$ is illustrated in Fig. 10, where $d_1(t) = [\sin(\frac{1}{10}t), \sin(\frac{1}{3}t), \sin(\frac{1}{5}t)]^T$. The responses of each controller to the disturbances are shown in Fig. 11.

For the $y$ direction, the steady-state responses by the conventional PID and LQR controllers exhibited oscillations

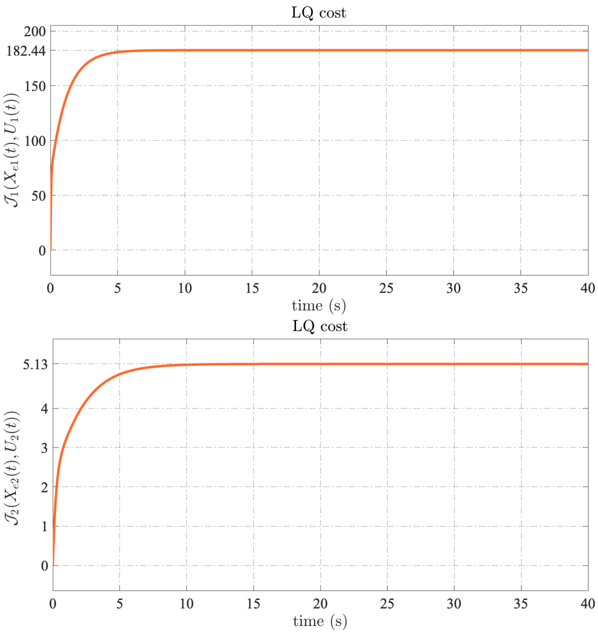


**FIGURE 9.** **LQ costs obtained from each subsystem controlled by the proposed RHGCC for the given initial values.**

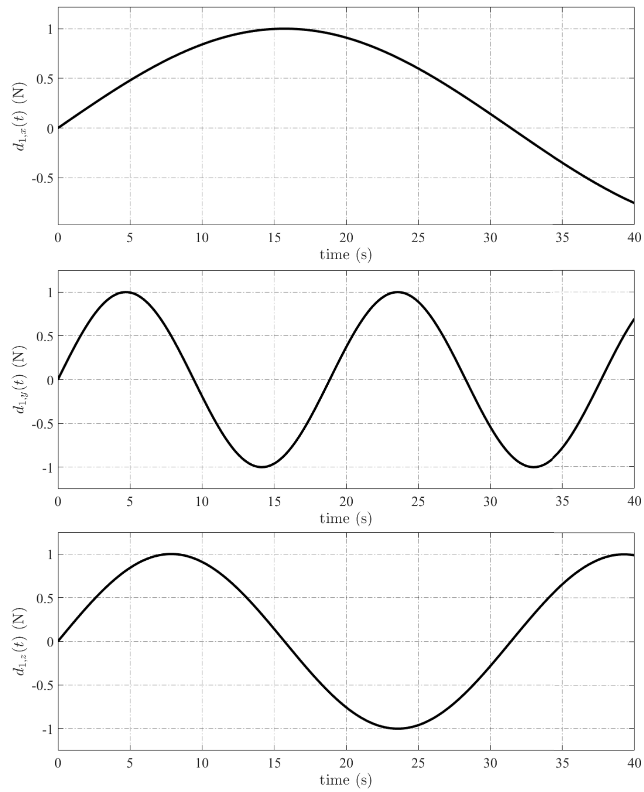


**FIGURE 10.** **Continuous disturbance inputs.**

with the magnitude of 1.12 m and 0.82 m peak to peak, respectively. On the other hand, the proposed RHGCC yields significantly reduced oscillation whose magnitude was 0.14 m peak to peak. Thus, the proposed RHGCC reduced the tracking errors in the $y$ direction by approximately 87.5% and 82.9% compared to the PID and LQR controllers, respectively. Similarly, in the $z$ direction, the steady-state response by the PID and LQR controllers presented oscillations with the magnitude of 1.01 m and 0.84 m peak to peak, respectively, whereas the response by the proposed RHGCC presented oscillations with a magnitude of 0.16 m peak to peak. Therefore, the proposed RHGCC reduced the tracking errors in the $z$ direction by approximately 84.2% and 81.0% compared to the PID and LQR controllers, respectively. Consistent with previous simulations, the proposed RHGCC significantly reduced the effect of disturbances, positioning the quadrotor UAV closer to the desired point compared to the conventional PID and LQR controllers. This demonstrates that the proposed RHGCC is much more robust against disturbances compared to conventional methods.

Additionally, the $H_\infty$ norms of each controller are calculated and shown in Fig. 12. For the given disturbances, the $H_\infty$ norm values of the PID and LQR controllers were calculated as 0.54 and 0.43, respectively, whereas the $H_\infty$ norm of the proposed RHGCC was calculated as 0.08. This represents 85.2% and 81.4% reductions compared to the PID and LQR controllers, respectively, highlighting that the proposed RHGCC significantly minimizes the impact of disturbances compared to the other controllers.

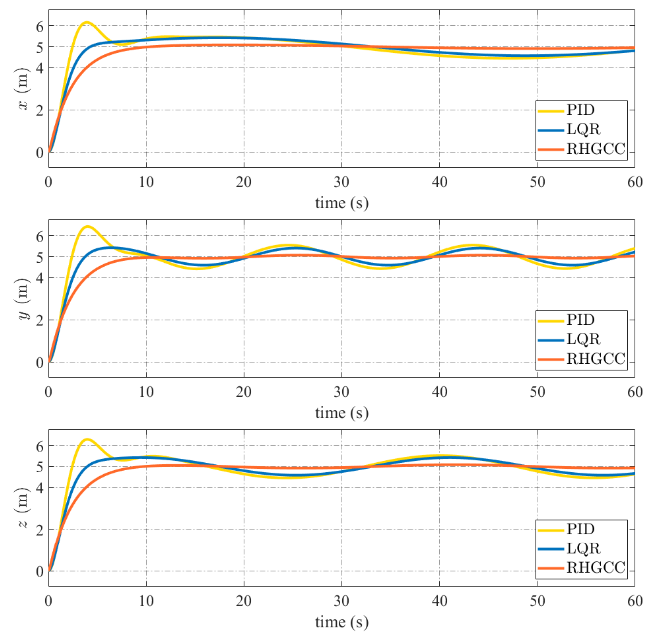


**FIGURE 11.** **Responses of each controller for position tracking when disturbances in Fig. 10 are applied.**

### *D. SIMULATION 3: COMPLEX DISTURBANCES*

In this subsection, we compare the $H_\infty$ norm and the response of each controller when continuous complex disturbances are applied. The introduced disturbance $d_1(t)$ is depicted in Fig. 13 and the disturbances are applied from 10 seconds after each controller's response reaches a steady state.

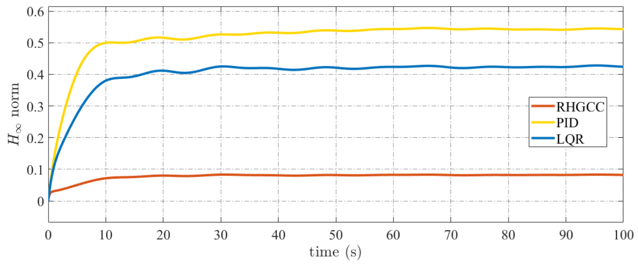


**FIGURE 12. Calculated $H_\infty$ norms from responses in Fig. 11 for each controller.**

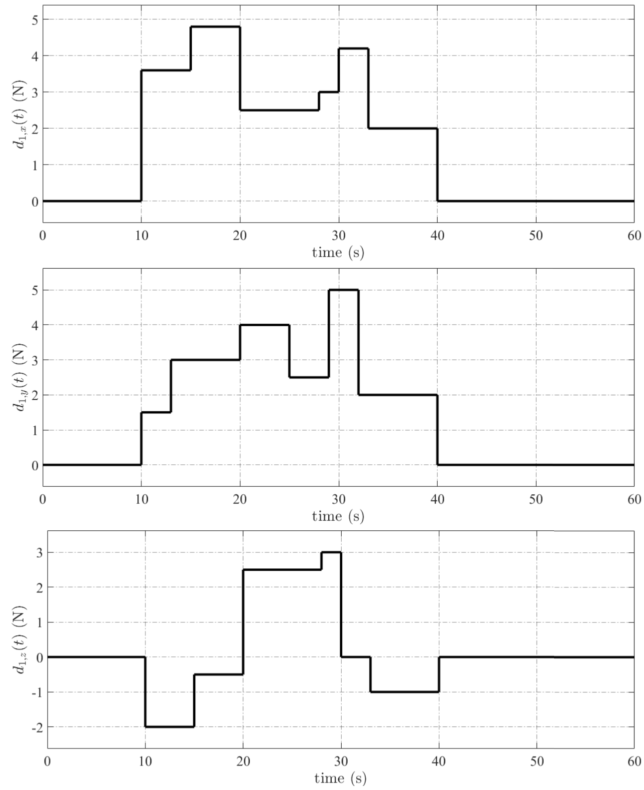


**FIGURE 13. Complex disturbance inputs.**

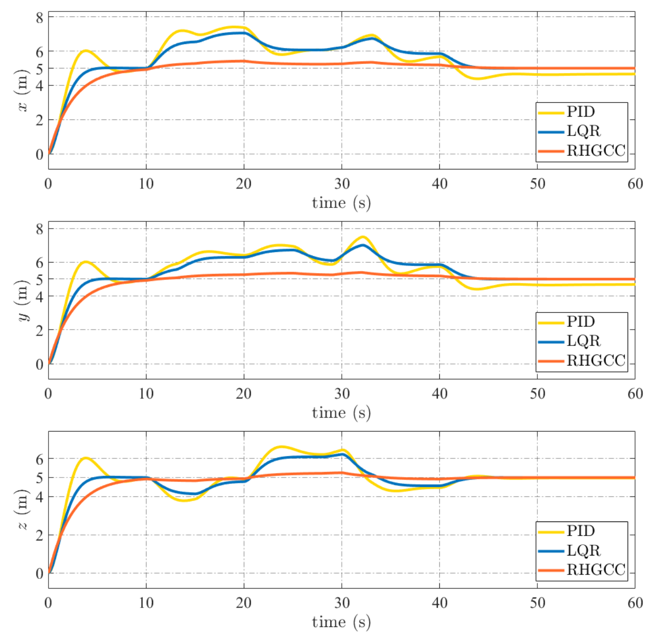


**FIGURE 14. Responses of each controller for position tracking when disturbances in Fig. 13 are applied.**

Fig. 14 depicts the responses of each controller when the disturbances in Fig. 13 are applied.

When examining the responses of each controller to disturbances in the $x$ direction over the entire time range, the conventional PID and LQR controllers exhibited oscillations with the magnitudes of 3.03 m and 2.06 m peak to peak, respectively, whereas the proposed RHGCC exhibited oscillations with a magnitude of 0.42 m peak to peak. In other words, the proposed RHGCC reduced the tracking errors due to disturbances by approximately 86.1% and 79.6% compared to the PID and LQR, respectively. In addition, in the $z$ direction, the PID and LQR controllers oscillated with peak-to-peak magnitudes of 2.82 m and 2.07 m, respectively. In contrast, the proposed RHGCC exhibited oscillations with a peak-to-peak magnitude of 0.42 m, resulting in a reduction of tracking errors of approximately 85.1% and 79.7% compared to the PID and LQR controllers, respectively. Similar to previous simulations, it is evident that the proposed RHGCC effectively reduces the impact of disturbances compared to other conventional controllers, positioning the quadrotor UAV closer to the desired point.

Additionally, the $H_\infty$ norms of each controller in this simulation are compared in Fig. 15. The $H_\infty$ norms of the PID and LQR controllers were calculated to be about 0.5 and 0.42, respectively, while that of the RHGCC was approximately 0.09. Compared to the conventional PID and LQR controllers, the $H_\infty$ norm of the proposed RHGCC is approximately 82.0% lower and 78.6% lower, respectively. Thus, the proposed RHGCC demonstrates notable robustness against disturbances compared to the conventional methods.

From the simulations, it is evident that the RHGCC proposed in this study significantly mitigates the impact of disturbances compared to other conventional control methods, effectively preserving the desired position and attitude under the presence of disturbances.

### *E. SIMULATION 4: EXPLORATION SCENARIOS WITH COMPLEX DISTURBANCES*

In this subsection, we compare the performance of each controller by assuming a scenario where the quadrotor UAV moves sequentially to given set points for exploration, with disturbances applied at specific locations. In this scenario, the quadrotor UAV takes off vertically to an altitude of 15 m from the starting point $\Pi_0 = [0, 0, 0]^T$ m and then flies around the entire building while maintaining 10 m from the outer wall to explore the exterior of a U-shaped building whose outer volume is 80 × 80 × 30 m, with an empty rectangular space

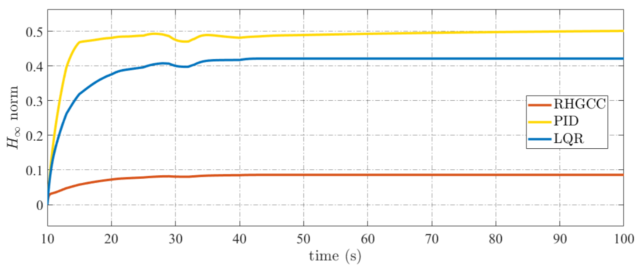


**FIGURE 15.** Calculated $H_\infty$ norms from responses in Fig. 14 for each controller.

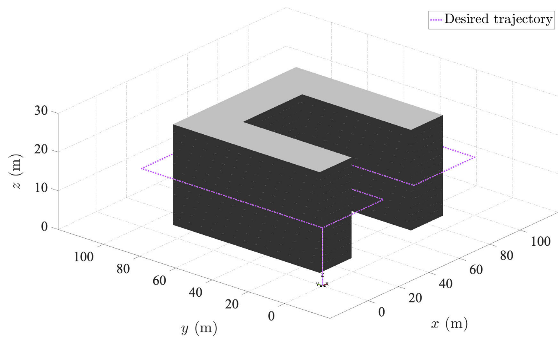


**FIGURE 16.** Appearance of the building being explored in the scenario by quadrotor UAV and the desired linear trajectory.

of 40 × 70 × 30 m in the middle of one side (Fig. 16). Finally, the quadrotor UAV lands at the starting point after exploring the perimeter of the building. Throughout the entire process, the quadrotor UAV sequentially reaches a total of 10 set-points ($\Pi_i, i \in \{1, \cdots, 10\}$), which are indicated in Fig. 17. Disturbances ($d_{1,j}(t), j \in \{1, \cdots, 7\}$) are applied at a total of 7 points ($\Pi_j^d, j \in \{1, \cdots, 7\}$), and Fig. 19 shows the locations where each disturbance is applied. The disturbances applied at each point are positional disturbances and are as follows:

- For 3 seconds at $\Pi_1^d = [0, 20, 15]^T$:
  $d_{1,1}(t) = [3\sin(\frac{1}{3}t - 117°), 0, 2\sin(\frac{1}{3}t) - 270°]^T$.
- For 0.5 seconds at $\Pi_2^d = [0, 100, 15]^T$:
  $d_{1,2}(t) = [-8\delta(t), 0, 0]^T$.
- For 1 seconds at $\Pi_3^d = [60, 100, 15]^T$:
  $d_{1,3}(t) = [0, 6\delta(t), 4\delta(t)]^T$.
- For 4 seconds at $\Pi_4^d = [100, 100, 15]^T$:
  $d_{1,4}(t) = [3\sin(\frac{1}{4}t - 270°), 3\sin(\frac{1}{4}t), 3\sin(\frac{1}{4}t)]^T$.
- For 0.5 seconds at $\Pi_5^d = [60, 40, 15]^T$:
  $d_{1,5}(t) = [0, 0, -10\delta(t)]^T$.
- For 2 seconds at $\Pi_6^d = [40, 60, 15]^T$:
  $d_{1,6}(t) = [\sin(\frac{1}{2}t + 198°) + 2, \sin(\frac{1}{2}t + 28.6°) + 1, \sin(\frac{1}{4}t + 58.3°) + 1]^T$.
- For 0.5 seconds at $\Pi_7^d = [30, 0, 15]^T$:
  $d_{1,7}(t) = [0, -3\delta(t), 5\delta(t)]^T$.

Here, $\delta(t)$ denotes the impulse function.

Fig. 18 depicts the responses by each controller against the applied disturbances mentioned above. Throughout the entire exploration, it can be seen that the proposed RHGCC significantly minimizes the impact of disturbances compared

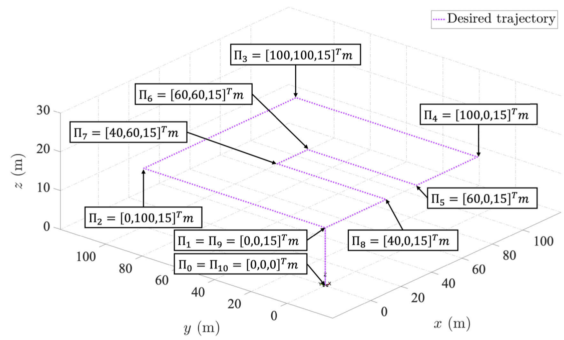


**FIGURE 17.** Set points given as input and the desired linear trajectory.

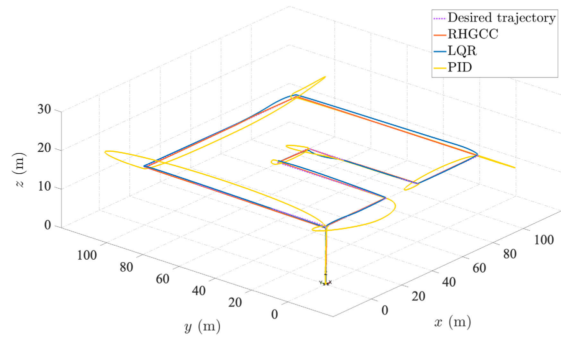


**FIGURE 18.** Responses of each controller for set point tracking when disturbances are applied at specific locations.

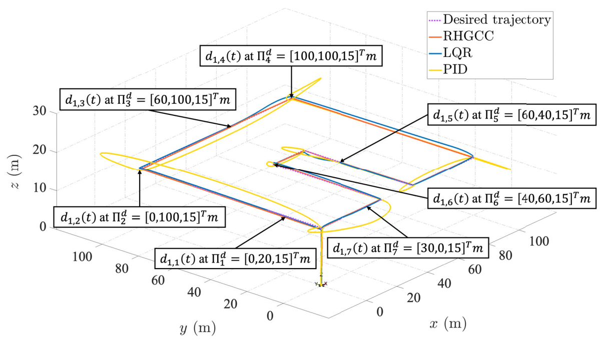


**FIGURE 19.** Locations where disturbances are applied and responses of each controller for set point tracking.

to the conventional PID and LQR controllers, enabling the quadrotor UAV to preserve the linear trajectory better while moving from the current set point to the desired next set point. Specifically, Fig. 20 is an enlarged view of certain section to qualitatively assess the effective disturbance suppression performance of the proposed RHGCC, showing the response of each controller when the disturbance $d_{1,5}(t)$ was applied at $\Pi_5^d$. For disturbances in the $z$ direction, the controlled response by the proposed method deviated by up to 0.17m from the desired value, whereas the responses by the PID and LQR controllers deviated by up to 1.39m and 0.86m from the desired position, respectively. This indicates that the proposed RHGCC reduced tracking

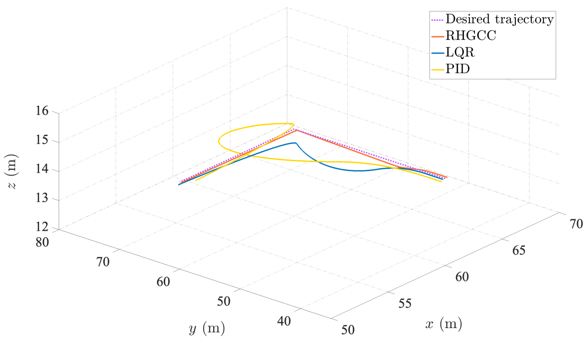


**FIGURE 20.** Enlarged view from Fig. 19 showing the responses of each controller for set point tracking when $d_{1,5}(t)$ is applied.

errors by approximately 87.8% and 80.2% compared to PID control and LQR, respectively. Therefore, the proposed method demonstrates notable robustness against disturbances compared to the conventional methods. Moreover, especially through the simulation in this subsection, it can be confirmed that the proposed RHGCC can significantly minimize the impacts of disturbances and effectively maintain the desired position and attitude, even under more complex scenarios with various disturbances that require tracking set points and preserving trajectory.

## V. CONCLUSION

In this study, we proposed the RHGCC for set-point tracking of the quadrotor UAV and a controller design method. The design process involved modeling the quadrotor UAV with a control system comprising an outer loop for position control and an inner loop for attitude control. First, for the closed-loop subsystems, performance analysis considering the LQ cost and $H_\infty$ norm was provided in terms of matrix inequalities. Then, the design method of the RHGCC for position and attitude control was proposed based on LMIs in the presence of model uncertainties and disturbances. The convex optimization problem was formulated aiming to minimize the LQ cost, guaranteeing the upper bound of $H_\infty$ norm. Through various simulations, it was illustrated that the proposed RHGCC significantly mitigated the influence of external disturbances while achieving a certain level of the LQ cost, distinguishing itself from conventional PID control and LQR. In future research, the design proposed in this study will be applied to a practical quadrotor UAV, and its performance will be validated through indoor and outdoor experiments.

## REFERENCES

[1] D. D. Dhadekar, P. D. Sanghani, K. K. Mangrulkar, and S. E. Talole, "Robust control of quadrotor using uncertainty and disturbance estimation," *J. Intell. Robotic Syst.*, vol. 101, no. 3, pp. 1–20, Mar. 2021.

[2] T. Hamel, R. Mahony, R. Lozano, and J. Ostrowski, "Dynamic modelling and configuration stabilization for an X4-flyer," *IFAC Proc. Volumes*, vol. 35, no. 1, pp. 217–222, 2002.

[3] S. A. H. Mohsan, N. Q. H. Othman, Y. Li, M. H. Alsharif, and M. A. Khan, "Unmanned aerial vehicles (UAVs): Practical aspects, applications, open challenges, security issues, and future trends," *Intell. Service Robot.*, vol. 16, pp. 109–137, Jan. 2023.

[4] M. Moshref-Javadi and M. Winkenbach, "Applications and research avenues for drone-based models in logistics: A classification and review," *Expert Syst. Appl.*, vol. 177, Sep. 2021, Art. no. 114854.

[5] W. H. Maes and K. Steppe, "Perspectives for remote sensing with unmanned aerial vehicles in precision agriculture," *Trends Plant Sci.*, vol. 24, no. 2, pp. 152–164, Feb. 2019.

[6] H. A. Foudeh, P. C. Luk, and J. F. Whidborne, "An advanced unmanned aerial vehicle (UAV) approach via learning-based control for overhead power line monitoring: A comprehensive review," *IEEE Access*, vol. 9, pp. 130410–130433, 2021.

[7] G. Sonugur, "A review of quadrotor UAV: Control and SLAM methodologies ranging from conventional to innovative approaches," *Robot. Auto. Syst.*, vol. 161, Mar. 2023, Art. no. 104342.

[8] W. Liu, Y. Ren, and F. Zhang, "Integrated planning and control for quadrotor navigation in presence of suddenly appearing objects and disturbances," *IEEE Robot. Autom. Lett.*, vol. 9, no. 1, pp. 899–906, Jan. 2024.

[9] H. Lee and H. J. Kim, "Trajectory tracking control of multirotors from modelling to experiments: A survey," *Int. J. Control, Autom. Syst.*, vol. 15, no. 1, pp. 281–292, Feb. 2017.

[10] T. Lee, M. Leok, and N. M. McClamroch, "Nonlinear robust tracking control of a quadrotor UAV on SE," *Asian J. Control.*, vol. 15, no. 2, pp. 391–408, 2013.

[11] J.-J. Xiong and E.-H. Zheng, "Position and attitude tracking control for a quadrotor UAV," *ISA Trans.*, vol. 53, no. 3, pp. 725–731, May 2014.

[12] Z. Xu, X. Nian, H. Wang, and Y. Chen, "Robust guaranteed cost tracking control of quadrotor UAV with uncertainties," *ISA Trans.*, vol. 69, pp. 157–165, Jul. 2017.

[13] B. Zhao, B. Xian, Y. Zhang, and X. Zhang, "Nonlinear robust adaptive tracking control of a quadrotor UAV via immersion and invariance methodology," *IEEE Trans. Ind. Electron.*, vol. 62, no. 5, pp. 2891–2902, May 2015.

[14] T. Dierks and S. Jagannathan, "Output feedback control of a quadrotor UAV using neural networks," *IEEE Trans. Neural Netw.*, vol. 21, no. 1, pp. 50–66, Jan. 2010.

[15] L. Martins, C. Cardeira, and P. Oliveira, "Linear quadratic regulator for trajectory tracking of a quadrotor," *IFAC-PapersOnLine*, vol. 52, no. 12, pp. 176–181, 2019.

[16] F. Kendoul, Z. Yu, and K. Nonami, "Guidance and nonlinear control system for autonomous flight of minirotorcraft unmanned aerial vehicles," *J. Field Robot.*, vol. 27, no. 3, pp. 311–334, May 2010.

[17] N. Cao and A. F. Lynch, "Inner–outer loop control for quadrotor UAVs with input and state constraints," *IEEE Trans. Control Syst. Technol.*, vol. 24, no. 5, pp. 1797–1804, Sep. 2016.

[18] X. Zhang, B. Xian, B. Zhao, and Y. Zhang, "Autonomous flight control of a nano quadrotor helicopter in a GPS-denied environment using on-board vision," *IEEE Trans. Ind. Electron.*, vol. 62, no. 10, pp. 6392–6403, Oct. 2015.

[19] S. Islam, P. X. Liu, and A. E. Saddik, "Robust control of four-rotor unmanned aerial vehicle with disturbance uncertainty," *IEEE Trans. Ind. Electron.*, vol. 62, no. 3, pp. 1563–1571, Mar. 2015.

[20] B. Zhou, B. Huang, Y. Su, and C. Zhu, "Interleaved periodic event-triggered communications-based distributed formation control for cooperative unmanned surface vessels," *IEEE Trans. Neural Netw. Learn. Syst.*, vol. 1, no. 1, pp. 1–13, Jan. 2024.

[21] H. Peng, B. Huang, M. Jin, C. Zhu, and J. Zhuang, "Distributed finite-time bearing-based formation control for underactuated surface vessels with levant differentiator," *ISA Trans.*, vol. 147, pp. 239–251, Apr. 2024.

[22] B. Zhou, B. Huang, Y. Su, W. Wang, and E. Zhang, "Two-layer leader-follower optimal affine formation maneuver control for networked unmanned surface vessels with input saturations," *Int. J. Robust Nonlinear Control*, vol. 34, no. 5, pp. 3631–3655, Mar. 2024.

[23] B. Huang, S. Song, C. Zhu, J. Li, and B. Zhou, "Finite-time distributed formation control for multiple unmanned surface vehicles with input saturation," *Ocean Eng.*, vol. 233, Aug. 2021, Art. no. 109158.

[24] U. Ansari, A. H. Bajodah, and M. T. Hamayun, "Quadrotor control via robust generalized dynamic inversion and adaptive non-singular terminal sliding mode," *Asian J. Control*, vol. 21, no. 3, pp. 1237–1249, May 2019.

[25] O. Mofid, S. Mobayen, C. Zhang, and B. Esakki, "Desired tracking of delayed quadrotor UAV under model uncertainty and wind disturbance using adaptive super-twisting terminal sliding mode control," *ISA Trans.*, vol. 123, pp. 455–471, Apr. 2022.

[26] D. Wang, Q. Pan, Y. Shi, J. Hu, and C. Zhao, "Efficient nonlinear model predictive control for quadrotor trajectory tracking: Algorithms and experiment," *IEEE Trans. Cybern.*, vol. 51, no. 10, pp. 5057–5068, Oct. 2021.

[27] B. Jiang, B. Li, W. Zhou, L.-Y. Lo, C.-K. Chen, and C.-Y. Wen, "Neural network based model predictive control for a quadrotor UAV," *Aerospace*, vol. 9, no. 8, p. 460, Aug. 2022.

[28] L. Xie, "Output feedback $H_\infty$ control of systems with parameter uncertainty," *Int. J. Control*, vol. 63, no. 4, pp. 741–750, Mar. 1996.

[29] X. Wang, B. Shirinzadeh, and M. H. Ang, "Nonlinear double-integral observer and application to quadrotor aircraft," *IEEE Trans. Ind. Electron.*, vol. 62, no. 2, pp. 1189–1200, Feb. 2015.

**BYEONGHWA LEE** received the B.S. degree in electronic engineering from the Kumoh National Institute of Technology, Gumi, South Korea, in 2024. He is currently pursuing the M.S. degree in engineering with Tokyo Institute of Technology, Tokyo, Japan. His research interests include optimal control, robust control, and power system control.

**DONGHO HYUN** received the B.S. degree in electronic engineering from the Kumoh National Institute of Technology, Gumi, South Korea, in 2024, where he is currently pursuing the M.S. degree in electronic engineering. His current research interests include power systems and frequency control.

**JUWON KIM** (Member, IEEE) received the B.S. degree in electronic engineering from the Kumoh National Institute of Technology, Gumi, South Korea, in 2024. He is currently pursuing the integrated degree with the Department of Electrical and Computer Engineering, Inha University, Incheon, South Korea. His research interests include multi-agent SLAM, robust sensing, multi sensor platform integration, and sensor fusion.

**SEUNGHWAN LEE** (Member, IEEE) received the B.S. degree in electronic engineering and computer sciences from Kyungpook National University, Daegu, South Korea, in 2008, and the M.S. and Ph.D. degrees in electrical engineering and computer sciences from Seoul National University, Seoul, South Korea, in 2010 and 2015, respectively. From 2015 to 2018, he was a Senior Researcher at the Samsung Electronics Mechatronics and Manufacturing Technology Center, Suwon, South Korea. He has been working with the School of Electronic Engineering, Kumoh National Institute of Technology, Gumi, South Korea, since 2018. He is currently working as an Associate Professor. His research interests include multi-robot SLAM, multi-robot coverage path planning, and human-like navigation.

**JAEPIL BAN** (Member, IEEE) received the Ph.D. degree in electrical engineering from Pohang University of Science and Technology, Pohang, South Korea, in 2020. From August 2020 to August 2021, he was a Postdoctoral Researcher at Pohang University of Science and Technology. Since 2021, he has been an Assistant Professor with the Kumoh National Institute of Technology. His research interests include robust and optimal control, hybrid systems, power system control, applications of reinforcement learning, and power system state and line parameter estimation.